

Black Hole and Galaxy Coevolution in Moderately Luminous Active Galactic Nuclei at $z \sim 1.4$ in SXDF

KENTA SETOGUCHI ¹, YOSHIHIRO UEDA ¹, YOSHIKI TOBA ^{1,2,3} AND MASAYUKI AKIYAMA ⁴

¹*Department of Astronomy, Kyoto University, Kitashirakawa-Oiwake-cho, Sakyo-ku, Kyoto 606-8502, Japan*

²*Academia Sinica Institute of Astronomy and Astrophysics, 11F of Astronomy-Mathematics Building, AS/NTU, No.1, Section 4, Roosevelt Road, Taipei 10617, Taiwan*

³*Research Center for Space and Cosmic Evolution, Ehime University, 2-5 Bunkyo-cho, Matsuyama, Ehime 790-8577, Japan*

⁴*Astronomical Institute, Tohoku University, 6-3 Aramaki, Aoba-ku, Sendai, Miyagi 980-8578, Japan*

(Received June 12, 2020; Revised January 22, 2021; Accepted January 22, 2021)

ABSTRACT

We investigate the relation of black hole mass versus host stellar mass and that of mass accretion rate versus star formation rate (SFR) in moderately luminous ($\log L_{\text{bol}} \sim 44.5 - 46.5 \text{ erg s}^{-1}$), X-ray selected broad-line active galactic nuclei (AGNs) at $z = 1.18 - 1.68$ in the Subaru/XMM-Newton Deep Field. The far-infrared to far-ultraviolet spectral energy distributions of 85 AGNs are reproduced with the latest version of Code Investigating GALaxy Emission (CIGALE), where the AGN clumpy torus model SKIRTOR is implemented. Most of their hosts are confirmed to be main sequence star-forming galaxies. We find that the mean ratio of the black hole mass (M_{BH}) to the total stellar mass (M_{stellar}) is $\log M_{\text{BH}}/M_{\text{stellar}} = -2.2$, which is similar to the local black hole-to-bulge mass ratio. This suggests that if the host galaxies of these moderately luminous AGNs at $z \sim 1.4$ are dominated by bulges, they already established the local black hole mass-bulge mass relation; if they are disk dominant, their black holes are overmassive relative to the bulges. AGN bolometric luminosities and SFR show a good correlation with ratios higher than that expected from the local black hole-to-bulge mass relation, suggesting that these AGNs are in a SMBH-growth dominant phase.

Keywords: Active galaxies (17) — Active galactic nuclei (16) — Supermassive black holes (1663)

1. INTRODUCTION

The evolution of supermassive black holes (SMBHs) and their host galaxies is one outstanding question in astrophysics. In the local universe ($z < 1$), a tight correlation between SMBH mass (M_{BH}) and galactic classical bulge mass (M_{bulge}) has been discovered (e.g., Magorrian et al. 1998; Marconi & Hunt 2003; Häring & Rix 2004; Gültekin et al. 2009; Kormendy & Ho 2013). This correlation indicates coevolution between SMBHs and their host galaxies (e.g., Kormendy & Ho 2013). A key population to unveil the origin of the coevolution is active galactic nuclei (AGNs) at cosmic noon ($z \sim 1 - 3$), when the bulk of the growth of SMBHs and galaxies took place (e.g., Madau & Dickinson 2014; Ueda et al. 2014; Aird et al. 2015). Using multiwavelength data in deep

survey fields, many authors investigated the relation between the AGN luminosity (or mass accretion rate onto the SMBH) and the star formation rate (SFR) of the host galaxy, which represent the mass growth rates of the SMBH and galaxy, respectively (e.g., Rosario et al. 2012; Stanley et al. 2015; Yang et al. 2017; Ueda et al. 2018; Yang et al. 2019; Aird et al. 2019; Stemo et al. 2020). The relation between the SMBH mass (M_{BH}) and host stellar mass (M_{stellar}) has been also studied for broad-line AGNs whose black hole masses were determined using the broad-line widths and continuum luminosities (e.g., Jahnke et al. 2009; Merloni et al. 2010; Suh et al. 2020). However, due to observational difficulties, studies based on spectroscopically measured M_{BH} are still limited. It is thus important to systematically study the relations among M_{BH} , AGN luminosity (or its ratio to M_{BH} , the Eddington ratio λ_{Edd}), M_{stellar} , and SFR using a highly complete AGN sample at cosmic noon.

The Subaru / *XMM-Newton* Deep Field (SXDF; Sekiguchi et al. 2005) is one of the best-studied deep multiwavelength survey fields. Ueda et al. (2008) presented the X-ray source catalog from the original 7 XMM-Newton pointings covering an area of 1.14 deg^2 , whose multiwavelength (radio, mid-IR to far-UV) properties were studied by Akiyama et al. (2015). The spectroscopic or photometric redshifts were available for all the objects. Nobuta et al. (2012) estimated the AGN luminosity at the rest-frame 3000 \AA ($L_{\lambda 3000}$) from the optical spectra, optical photometries, or X-ray luminosities and derived M_{BH} and Eddington ratios of broad-line AGNs at $z \sim 1.4$ from the line widths of Mg II or H α lines and continuum luminosities ($L_{\lambda 3000}$) in the spectroscopic survey data². The rich multiwavelength photometric datasets and the highly complete catalog of black hole masses available for broad-line AGNs at $z = 1.18 - 1.68$ provide us with an ideal opportunity to study the relations among physical properties of the AGN and host galaxies at these redshifts.

The structure of this paper is as follows. We describe the details of sample selection and the method of the spectral energy distribution (SED) fitting in Section 2. To better estimate the SFRs, we add far-infrared (FIR) photometric data by cross-matching with the *Herschel* Multi-tiered Extragalactic Survey (HerMES) catalog (Oliver et al. 2012). In Section 3 we perform correlation analysis between M_{BH} and M_{stellar} and that between SFR and L_{bol} (or λ_{Edd}). The results are discussed in comparison with previous works. The conclusions are summarized in Section 4. Throughout this paper, the adopted cosmology is a flat universe with $H_0 = 70 \text{ km s}^{-1} \text{ Mpc}^{-1}$, $\Omega_M = 0.3$, and $\Omega_\Lambda = 0.7$.

2. DATA AND ANALYSIS

2.1. Sample Selection

To investigate statistical properties of AGNs at $z \sim 1.4$, we selected those at $z = 1.18 - 1.68$ in the SXDF detected with XMM-Newton (Ueda et al. 2008) and identified with multiwavelength catalogs (Akiyama et al. 2015). Among the 117 at $z = 1.18 - 1.68$ broad-line AGNs in the Akiyama et al. (2015) catalog, black hole masses of 116 AGNs were measured by Nobuta et al. (2012), which constitute our parent sample. The 3000 \AA monochromatic luminosities range from $\log \lambda_{3000} L_{\lambda 3000} = 43.6$ to 47.3 erg s^{-1} with a median of 44.7 erg s^{-1} . The Eddington ratios were calcu-

lated as $\lambda_{\text{Edd}} = L_{\text{bol}}/L_{\text{Edd}}$, where $L_{\text{bol}} = 5.8 \lambda_{3000} L_{\lambda 3000}$ (Richards et al. 2006) and $L_{\text{Edd}} = 1.25 \times 10^{38} M_{\text{BH}}/M_\odot$. The black hole masses and Eddington ratios range $\log M_{\text{BH}}/M_\odot = 7.2 \sim 9.8$ (median 8.4) and $\log \lambda_{\text{Edd}} = -2.06 \sim 0.13$ (median -1.1), respectively (Nobuta et al. 2012).

2.2. Cross-match with FIR Data from HerMES

Since FIR data are important to estimate the SFRs of the host galaxies, we added FIR photometries obtained by HerMES (Oliver et al. 2012) to the multiwavelength SEDs in Akiyama et al. (2015). Using the HerMES DR4 catalog in the XMM-LSS field, we performed nearest-neighbor matching within a search radius of $20''$ around the optical counterparts of the X-ray sources. We identified 80, 78, and 65 *Herschel* counterparts at 250, 350, and $500 \mu\text{m}$, respectively. For non-detected sources, we assign 3σ upper limits of 15.48, 12.72, and 18.48 mJy at 250, 350, and $500 \mu\text{m}$, respectively (Oliver et al. 2012).

Since *Herschel*/SPIRE has a large beam size (full widths at half maximum (FWHM) of $18.2''$, $24.9''$, $36.3''$ at 250, 350, and $500 \mu\text{m}$, respectively; Oliver et al. 2012), the measured FIR photometries may be contaminated by nearby sources. To evaluate the effect, we checked the image at $24 \mu\text{m}$, the closest band to the *Herschel* ones, utilizing the Spitzer UKIDSS Ultra Deep Survey (SpUDS) catalog and the Spitzer Wide-Area Infrared Extragalactic (SWIRE) legacy survey catalog (Lonsdale et al. 2003, 2004). We searched for $24 \mu\text{m}$ sources within a radius of $18.2''$ (i.e., the half of the FWHM at $500 \mu\text{m}$) around the position of the optical counterpart. We found that 26 out of the 116 objects have multiple counterparts in the $24 \mu\text{m}$ band. For these sources, we calculated the 3σ upper boundary of the FIR photometries and used them as the upper limits.

2.3. SED Fitting with CIGALE

We performed a multi-component SED fitting to 19 photometries (or their upper limits) in the far-IR (*Herschel*/SPIRE and PACS), mid-IR (Spitzer/IRAC and MIPS), near-IR (UKIDSS), optical (Subaru), and ultraviolet (GALEX) bands for each object (see Table 1 of Akiyama et al. 2015 for details except for the far-IR data).

We employed a new version of Code Investigating GALaxy Emission (CIGALE; Burgarella et al. 2005; Noll et al. 2009; Boquien et al. 2019), named X-CIGALE (Yang et al. 2020), where a clumpy two-phase torus model, SKIRTOR (Stalevski et al. 2016), has been implemented as an AGN template. An advantage of CIGALE is that re-emission from dust in the mid-IR and far-IR bands is self-consistently calculated by considering the energy

¹ See Kocevski et al. (2018) for the Chandra catalog, which covers a 0.33 deg^2 area with deeper flux limits.

² See also Oh et al. (2019) for additional measurements of M_{BH} at different redshifts.

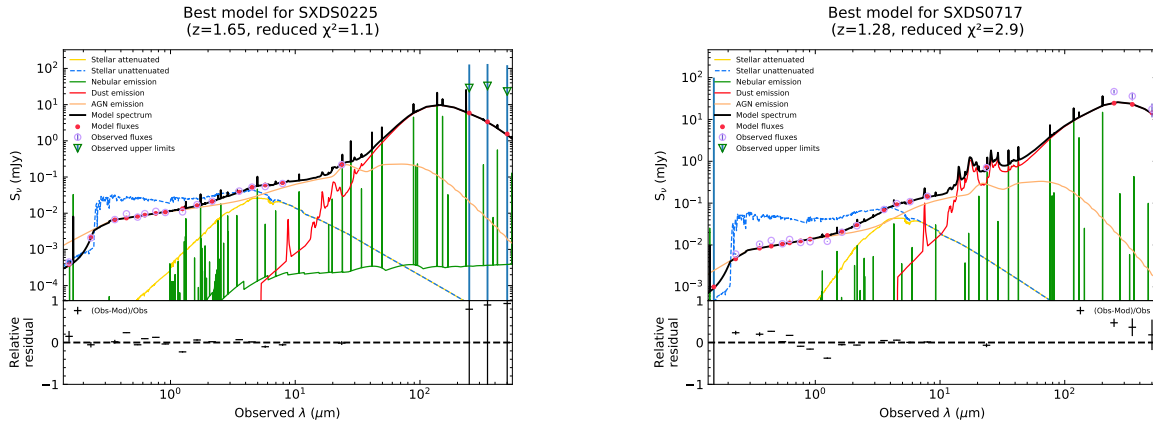


Figure 1. Examples of the SED fitting for our objects with CIGALE. SXDS0225 (left) and SXDS0717 (right) are a quasar and a Seyfert, respectively. The black solid lines display the best-fit SEDs.

balance. Following Toba et al. (2019b), we adopted a star formation history (SFH) of two exponentially-decreasing SFRs with different e-folding times: the main stellar population (τ_{main}) and the late starburst one (τ_{burst}). We chose the single stellar population (SSP) model (Bruzual & Charlot 2003), assuming a Chabrier initial mass function (IMF; Chabrier 2003). The nebular emission model is based on Inoue (2011), for which we used the default template and parameters. Dust attenuation was taken into account with the law of Calzetti et al. (2000), parameterized by the color excess ($E(B - V)_*$). The reprocessed IR emission of dust absorbed from UV/optical stellar emission is modeled by using dust templates provided by Dale et al. (2014). For AGN emission, we utilized the SKIRTOR model that has 7 parameters: torus optical depth at $9.7 \mu\text{m}$ ($\tau_{9.7}$), torus density radial parameter (p), torus density angular parameter (q), angle between the equatorial plane and edge of the torus (Δ), ratio of the maximum to minimum radii of the torus ($R_{\text{max}}/R_{\text{min}}$), the viewing angle (θ), and the AGN fraction in total IR luminosity (f_{AGN}). In order to avoid a degeneracy of AGN templates in the same manner as Yang et al. (2020), we fixed $R_{\text{max}}/R_{\text{min}}$, Δ , and θ that are optimized for type 1 AGNs. Table 1 summarizes the free parameters in the SED model. We note that CIGALE can handle the upper limits of photometries to perform Bayesian estimation, utilizing the method by Sawicki (2012) (see Section 4.3 in Boquien et al. 2019, for more detail).

We found that X-CIGALE adequately reproduced the SEDs from far-IR ($500 \mu\text{m}$) to far-UV (1500 \AA) in a majority of objects; among the 116 objects, 92 had reduced $\chi^2 < 10.0$. As a sanity check, we compared the AGN luminosity obtained from X-CIGALE and L_{bol} estimated by Nobuta et al. (2012). It is found that 7 out of the 92 objects show significantly smaller AGN luminosities in

Table 1. Free Parameters used for the SED fitting of our objects with CIGALE.

Parameter	Value
Double exp. SFH	
τ_{main} [Myr]	1000, 3000, 4000, 8000
τ_{burst} [Myr]	3, 8, 80
f_{burst}	0.001, 0.1, 0.3
age [Myr]	1000, 4000, 6000
Single stellar population (Bruzual & Charlot 2003)	
IMF	Chabrier (2003)
Metallicity	0.02
Dust attenuation (Calzetti et al. 2000)	
$E(B - V)_*$	0.01, 0.1, 0.2, 0.3, 0.4, 0.5, 0.6, 0.7, 0.8, 1.0
Dust emission (Dale et al. 2014)	
IR power-law slope (α_{dust})	0.0625, 1.0000, 1.5000, 2.0000, 2.5000, 3.0000, 4.0000
AGN emission (Stalevski et al. 2016)	
$\tau_{9.7}$	3, 7
p	0.0, 1.0
q	0.0, 1.0
Δ	40°
$R_{\text{max}}/R_{\text{min}}$	30
θ	30°
f_{AGN}	0.1, 0.3, 0.5, 0.7, 0.9

X-CIGALE. Detailed inspection suggests that these 7 objects are likely weakly-absorbed AGNs, whose SEDs cannot be well reproduced with the current AGN template in X-CIGALE. We thus excluded them from the sample and used the remaining 85 objects in the following analysis. Examples of our SED fitting for two objects are shown in Figure 1.

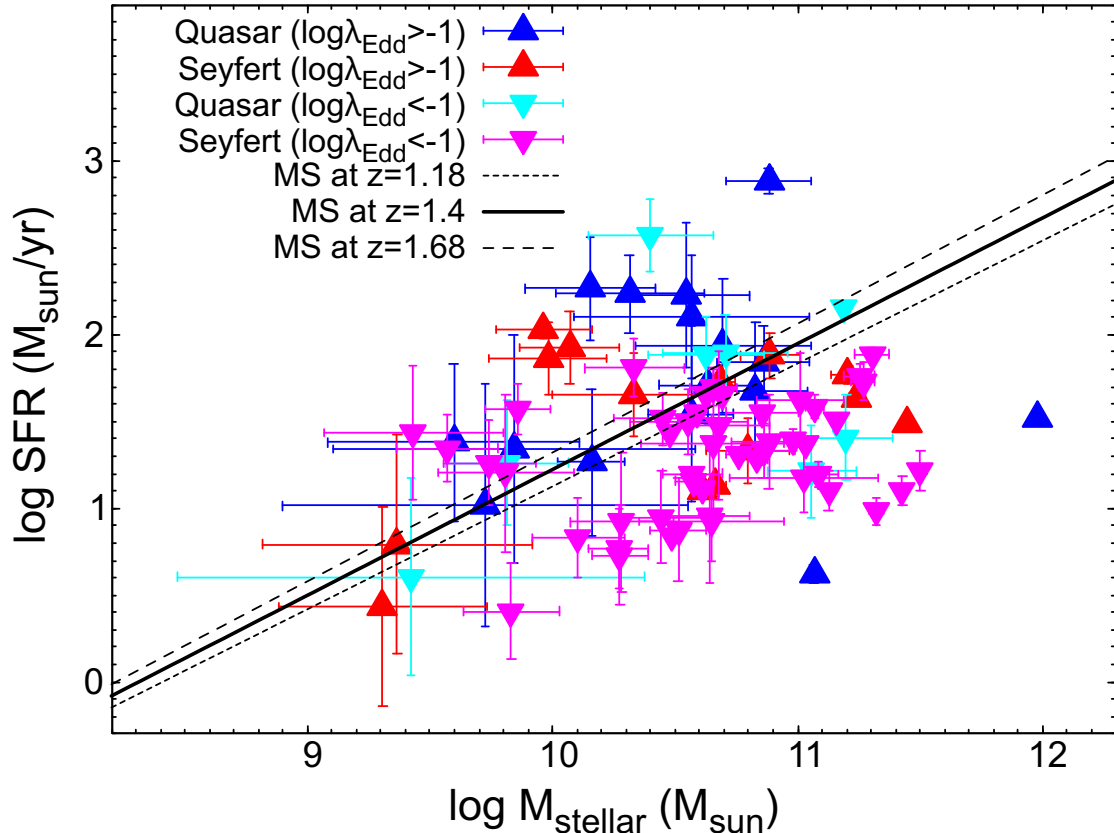


Figure 2. M_{stellar} vs. SFR of our objects. The black solid line represents the main sequence relation at $z = 1.4$ from Speagle et al. (2014). The large blue triangles: quasars ($\log L_{\text{bol}}/L_{\odot} > 12$) with $\log \lambda_{\text{Edd}} > -1$. The large red triangles: Seyferts ($\log L_{\text{bol}}/L_{\odot} < 12$) with $\log \lambda_{\text{Edd}} > -1$. The cyan inverse triangles: quasars with $\log \lambda_{\text{Edd}} < -1$. The magenta inverse triangles: Seyferts with $\log \lambda_{\text{Edd}} < -1$.

To check whether their physical properties are reliably estimated given the uncertainties of the photometries, we performed a mock analysis implemented on X-CIGALE. It enables us to compare the parameters estimated by X-CIGALE using the real catalog with those from the mock catalog, which X-CIGALE produces from the best-fit SED and photometric errors for each object (see, e.g., Boquien et al. 2019; Yang et al. 2020; Toba et al. 2020 for more detail). We confirmed that our M_{stellar} and SFR values adequately agree with those obtained from the mock catalog within the errors.

3. RESULTS AND DISCUSSIONS

3.1. Results of the SED with CIGALE

In this paper, we focus on the SFR and the total stellar mass (including those of the bulge [M_{bulge}] and the galactic disk) of the host galaxies derived from our SED fitting. We then compare them with the AGN parameters, L_{bol} , M_{BH} , and λ_{Edd} . For convenience, we divide our sample into four groups by the bolometric luminosity and Eddington ratio and use different sym-

bols commonly in all plots. We refer to those with $\log L_{\text{bol}}/L_{\odot} > 12$ and $\log L_{\text{bol}}/L_{\odot} < 12$ as quasars and Seyferts, respectively, and those with $\log \lambda_{\text{Edd}} > -1$ and $\log \lambda_{\text{Edd}} < -1$ as high Eddington AGNs and low Eddington ones, respectively.

3.2. Stellar Mass and SFR

Figure 2 displays the relation between M_{stellar} and SFR of our sample. The stellar masses and SFRs of our sample range from $\log M_{\text{stellar}}/M_{\odot} = 9.3$ to 12.0 (median 10.6) and from $\log \text{SFR}/(M_{\odot} \text{ yr}^{-1}) = 0.4$ to 2.9 (median 1.4), respectively. The black solid line represents the main sequence (MS) relation at $z = 1.4$ given by Speagle et al. (2014). As noticed, most of the host galaxies are classified as star forming galaxies in the MS; only a very small fraction are starburst galaxies (>0.6 dex above the MS line). This result is consistent with previous studies of X-ray selected AGNs with similar luminosities and redshifts (e.g., Santini et al. 2012; Yang et al. 2017; Ueda et al. 2018).

3.3. Stellar Mass versus Black Hole Mass

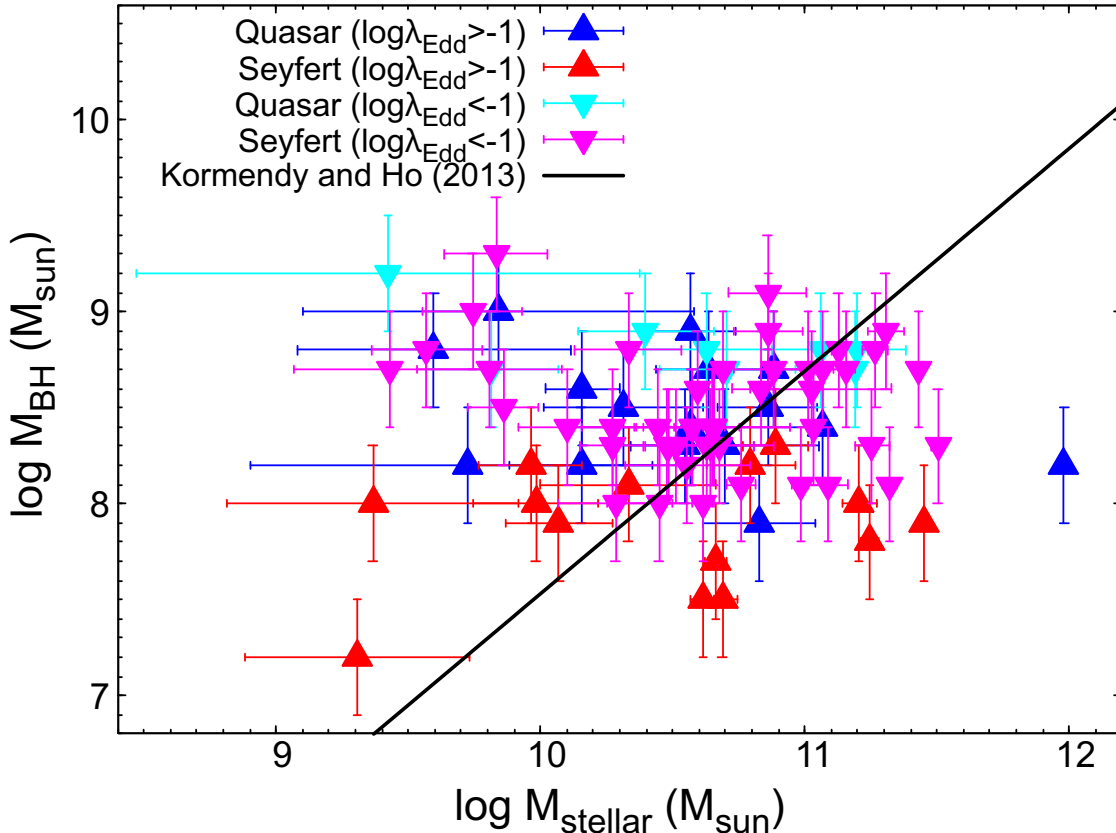


Figure 3. Relation between M_{stellar} and M_{BH} . The symbols are the same as in Figure 2. The black solid line represents the local black hole-to-bulge mass ratio from Kormendy & Ho (2013).

Figure 3 plots the relation between M_{stellar} and M_{BH} . We perform a correlation analysis with the method of Kelly (2007) where the errors in the two parameters are taken into account (see also Toba et al. 2019a for an application to a large number of X-ray selected type 1 AGNs). It yields a correlation coefficient of $r = -0.068 \pm 0.204$, indicating no correlation. This would be simply due to the small range of M_{BH} in our sample. A mean $M_{\text{BH}}/M_{\text{stellar}}$ ratio is calculated to be -2.2 with a 1σ scatter of 0.69. The black solid line represents the local M_{BH} versus M_{bulge} relation for classical bulges determined by Kormendy & Ho (2013). On average, our sample has $M_{\text{BH}}/M_{\text{stellar}}$ ratios similar to the local $M_{\text{BH}}/M_{\text{bulge}}$ relation. Since $M_{\text{stellar}} \geq M_{\text{bulge}}$, the $M_{\text{BH}} - M_{\text{bulge}}$ relation for disk-dominant galaxies is different from the local one in the sense that black holes are overmassive.

Our result on the $M_{\text{BH}}/M_{\text{stellar}}$ ratio at $1.18 < z < 1.68$ is consistent with that reported by Merloni et al. (2010) for type-1 AGNs with similar bolometric luminosities at $1 < z < 2.2$ in the COSMOS field (after converting M_{stellar} from a Salpeter IMF to a Chabrier IMF by -0.255 dex). Although Merloni et al. (2010)

argued that the $M_{\text{BH}}/M_{\text{stellar}}$ ratio evolves with $(1+z)^{1.15 \pm 0.13}$ (for a Chabrier IMF) compared with the local $M_{\text{BH}}/M_{\text{bulge}}$ relation by Häring & Rix (2004), the recent upward correction by Kormendy & Ho (2013) in the local $M_{\text{BH}}/M_{\text{bulge}}$ ratio by ~ 0.5 dex would indicate no evolution from $z = 0$ to $z \sim 1.4$. More recently, however, Suh et al. (2020) obtained a significantly lower ratio ($\log M_{\text{BH}}/M_{\text{stellar}} \approx -2.7$) than our result for AGNs at similar redshifts detected in the Chandra COSMOS Legacy Survey, adopting a Chabrier IMF (i.e., the same as our IMF). Their mean M_{stellar} value is ~ 0.5 dex larger than our result, whereas AGN bolometric luminosities of their sample are typically ~ 0.5 dex smaller than ours. The reason behind the discrepancy is unclear; it is most likely caused by different models used in the SED fitting. Indeed, Suh et al. (2019) obtained more massive stellar masses in type-1 AGNs than in type-2 AGNs at the same redshifts. In this paper, we do not pursue this issue further, but we always need to bear these possible systematic uncertainties in mind.

Our result suggests that (1) moderately luminous AGNs at $z \sim 1.4$ with bulge-dominant galaxies already established the local $M_{\text{BH}}-M_{\text{bulge}}$ relation and

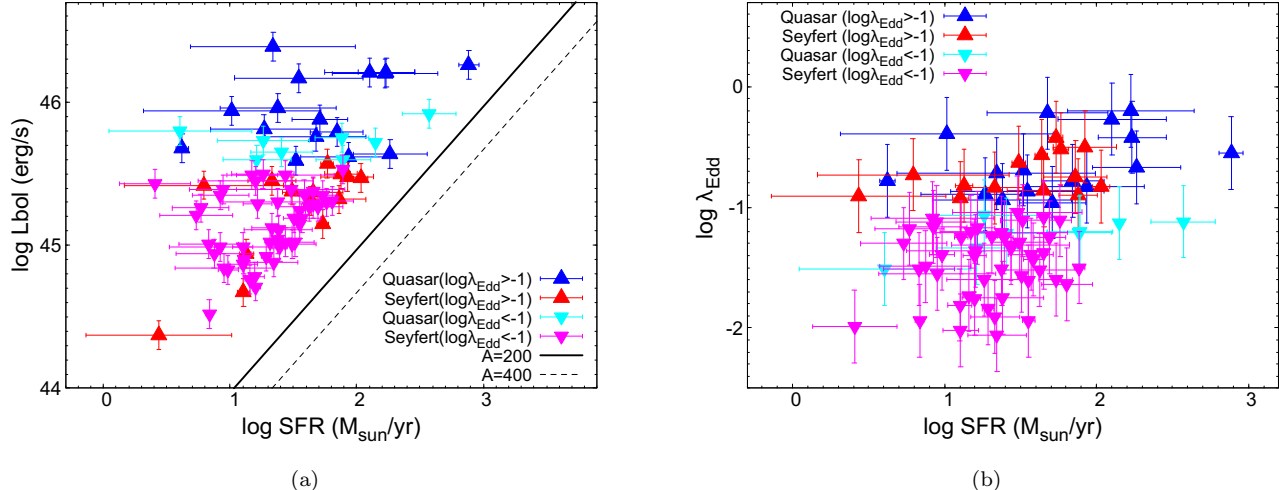


Figure 4. Relations between (a) SFR and L_{bol} and (b) SFR and λ_{Edd} . The symbols are the same as in Figure 2. The black solid and dashed lines in (a) correspond to equation (1) with $A = 200$ and $A = 400$, respectively.

that (2) those with disk-dominant galaxies have over-massive SMBHs relative to the bulge stellar masses. This implies that, in the disk-dominant galaxies, later star formation in the bulge at $z \lesssim 1.4$ caught up the earlier growth of the SMBH or that the mass of the disk was redistributed into the bulge by mergers or disk instabilities at $z \lesssim 1.4$ (see, e.g., Jahnke et al. 2009). Such a tendency has been reported by many authors for luminous AGNs at the same or higher redshifts (see Kormendy & Ho 2013 and references therein). It is, however, likely to be subject to selection bias toward luminous AGNs. It is possible that lower-luminosity AGNs may have less massive SMBHs (e.g., Ueda et al. 2018; Izumi et al. 2019). Hence, the overall picture of SMBH and galaxy coevolution is still an open question (see Section 3.5 for discussion).

3.4. SFR versus Black Hole Accretion Rate and Eddington Ratio

Figure 4 (a) shows the relation between SFR and L_{bol} , which represent the time derivatives of M_{stellar} and M_{BH} at the observed epoch. We obtain a correlation coefficient of $r = 0.717 \pm 0.084$, indicating a significant positive correlation. The black solid and dashed lines correspond to the local $M_{\text{BH}}\text{-vs-}M_{\text{bulge}}$ and $M_{\text{BH}}\text{-vs-}M_{\text{stellar}}$ relations, respectively, that would be expected from exactly simultaneous evolution of SMBHs and their host galaxies. They are given as

$$\text{SFR} \times (1 - R) = A \times L_{\text{bol}}(1 - \eta)/\eta c^2, \quad (1)$$

where $R = 0.41$ (for a Chabrier IMF) is the return fraction, A the local star-to-SMBH mass ratio ($A = M_{\text{bulge}}/M_{\text{BH}} = 200$ or $A = M_{\text{stellar}}/M_{\text{BH}} = 400$), $\eta = 0.05$ the radiation efficiency, and c the light speed

(see Ueda et al. 2018). Our objects are located above these lines, indicating that they are in a SMBH-growth dominant phase.

Yang et al. (2017) show that the mean ratio of host galaxy SFR to AGN luminosity increases with redshift (see also, e.g., Stemo et al. 2020 for similar results). Generally, a flux-limited sample obtained from a single survey contains more luminous AGNs at higher redshifts. Then, even if there were no intrinsic correlation at a given redshift, the redshift dependence on the SFR-to- L_{bol} ratio could drive an apparent correlation between SFR and L_{bol} based on a sample that covers a wide redshift range. Thanks to the narrow redshift range of our sample ($z = 1.18 - 1.68$), however, the effect is estimated to be negligible compared with the observed scatter in the L_{bol} -to-SFR ratio. Yang et al. (2017) and Stemo et al. (2020) also report that the correlation between SFR and mass accretion rate (L_{bol}) comes from that between M_{stellar} and L_{bol} and the main sequence M_{stellar} -SFR relation. However, we obtain a correlation coefficient between M_{stellar} and L_{bol} of $r = -0.037 \pm 0.142$ (no significant correlation), suggesting that the SFR- L_{bol} correlation is a primary one.

We note that this result is subject to selection biases toward luminous AGNs, similar to the case of the M_{stellar} versus M_{BH} relation. In fact, deeper Chandra surveys detected a dominant AGN population whose mass accretion rate-to-SFR ratios are smaller than the local relation (e.g., Yang et al. 2017, Ueda et al. 2018). The large scatter would be explained by time variability of AGN activities (Hickox et al. 2014) and/or non-coevolution nature for disk-dominated systems (Kormendy & Ho 2013). Yang et al. (2019) report that the average black hole accretion rate of all bulge-dominant galaxies

at $0.5 < z < 3.0$ shows a good correlation with the SFR, whereas disk-dominant ones do not.

We also plot the relation between SFR and λ_{Edd} in Figure 4(b). We obtain a correlation coefficient of $r = 0.623 \pm 0.136$. This indicates a similarly strong positive correlation to that between SFR and L_{bol} , as expected from a narrow range of M_{BH} (Figure 4). To our knowledge, this is the first report of such correlation based on direct measurements of M_{BH} for $z \sim 1.4$ AGNs (see Zhuang & Ho 2020 for the result for nearby AGNs at $z < 0.35$). Aird et al. (2019) show that high SFR galaxies tend to contain more AGNs with high "specific" accretion rates (those divided by their host stellar masses, instead of the black hole masses). That trend is not surprising given a moderate scatter between M_{BH} and M_{stellar} as shown in Figure 3.

We investigate whether the observed correlation between SFR and λ_{Edd} arises from that between SFR and L_{bol} given the small M_{BH} range. Following Zhuang & Ho (2020), we divide our sample by L_{bol} into two groups, quasars and Seyferts. The correlation coefficients between SFR and λ_{Edd} are found to be $r = 0.476 \pm 0.358$ (quasars) and $r = 0.581 \pm 0.179$ (Seyferts). Alternatively, when we divide the sample by λ_{Edd} , we obtain correlation coefficients between SFR and L_{bol} of $r = 0.634 \pm 0.167$ and $r = 0.743 \pm 0.115$ for high and low Eddington rate AGNs, respectively. The more significant correlations between SFR and L_{bol} than those between SFR and λ_{Edd} suggest that L_{bol} is likely to be the primary parameter. Zhuang & Ho (2020) have reached a similar conclusion for $z < 0.35$ AGNs.

3.5. Evolution of Black Hole-to-Stellar Mass Ratio

The SMBH-to-stellar mass ratio gives us a hint on the evolutionary scenario of our sample, in particular, whether the SMBHs grew earlier or later than the galaxies. Figure 5 (a) and (b) plots the mass ratio against L_{bol} and SFR, respectively. We obtain a correlation coefficient between L_{bol} and $M_{\text{BH}}/M_{\text{stellar}}$ of $r = 0.324 \pm 0.138$ and that between SFR and $M_{\text{BH}}/M_{\text{stellar}}$ of $r = -0.019 \pm 0.161$. The positive correlation of the SMBH-to-stellar mass ratio with the AGN luminosity but not with SFR prefers an evolutionary scenario where star formation precedes SMBH growth (as proposed by, e.g., Ueda et al. 2018) in the moderately luminous AGN phase; the reason why the correlation between SFR and $M_{\text{BH}}/M_{\text{stellar}}$ is unseen may be explained by the pres-

ence of the luminous quasars that show small SFR-to- L_{bol} ratios in the final stage of black hole mass growth. Our scenario predicts that the ratio of the black hole mass accretion rate to SFR increases with time during the moderately luminous AGN phase and hence should correlate with the SMBH-to-stellar mass ratio. Figure 5 (c) plots $M_{\text{BH}}/M_{\text{stellar}}$ against $L_{\text{bol}}/\text{SFR}$. They show a weak positive correlation ($r = 0.294 \pm 0.164$), which is in line with this picture.

4. CONCLUSION

We have applied the X-CIGALE code (Yang et al. 2020) to the far IR to far UV SED of moderately luminous ($\log L_{\text{bol}} \sim 44.5 - 46.5$), X-ray selected broad-line AGNs at $z = 1.18 - 1.68$ in the SXDF. The main conclusions are summarized as follows.

- The mean ratio of the black hole mass to the total stellar mass for a Chabrier IMF (including that in the bulge and disk) is found to be -2.2 , which is similar to the local SMBH-to-bulge mass ratio. This suggests that if the host galaxies of these moderately luminous AGNs at $z \sim 1.4$ are dominated by bulges, they already established the local SMBH mass-bulge mass relation; if they are dominated by disks, their SMBHs are overmassive relative to the bulges. However, a selection bias for luminous AGNs must be taken into account to discuss the properties of the whole galaxy population.
- We find a good correlation between AGN bolometric luminosities and SFR with ratios higher than that expected from the local $M_{\text{BH}} - M_{\text{bulge}}$ relation, suggesting that these AGNs are in a SMBH-growth dominant phase.

ACKNOWLEDGMENTS

We acknowledge the anonymous referee for careful reading of this paper and constructive feedback. We are deeply thankful to Prof. Veronique Buat, Dr. Guang Yang, and Prof. Denis Burgarella for helping to install X-CIGALE code. This work was financially supported by the Grant-in-Aid for Scientific Research grant Nos. 20H01946 (Y.U.), 18J01050, and 19K14759 (Y.T.).

REFERENCES

- Aird, J., Coil, A. L., Georgakakis, A., et al. 2015, MNRAS, 451, 1892
- Aird, J., Coil, A. L., Georgakakis, A., et al. 2019, MNRAS, 484, 4360

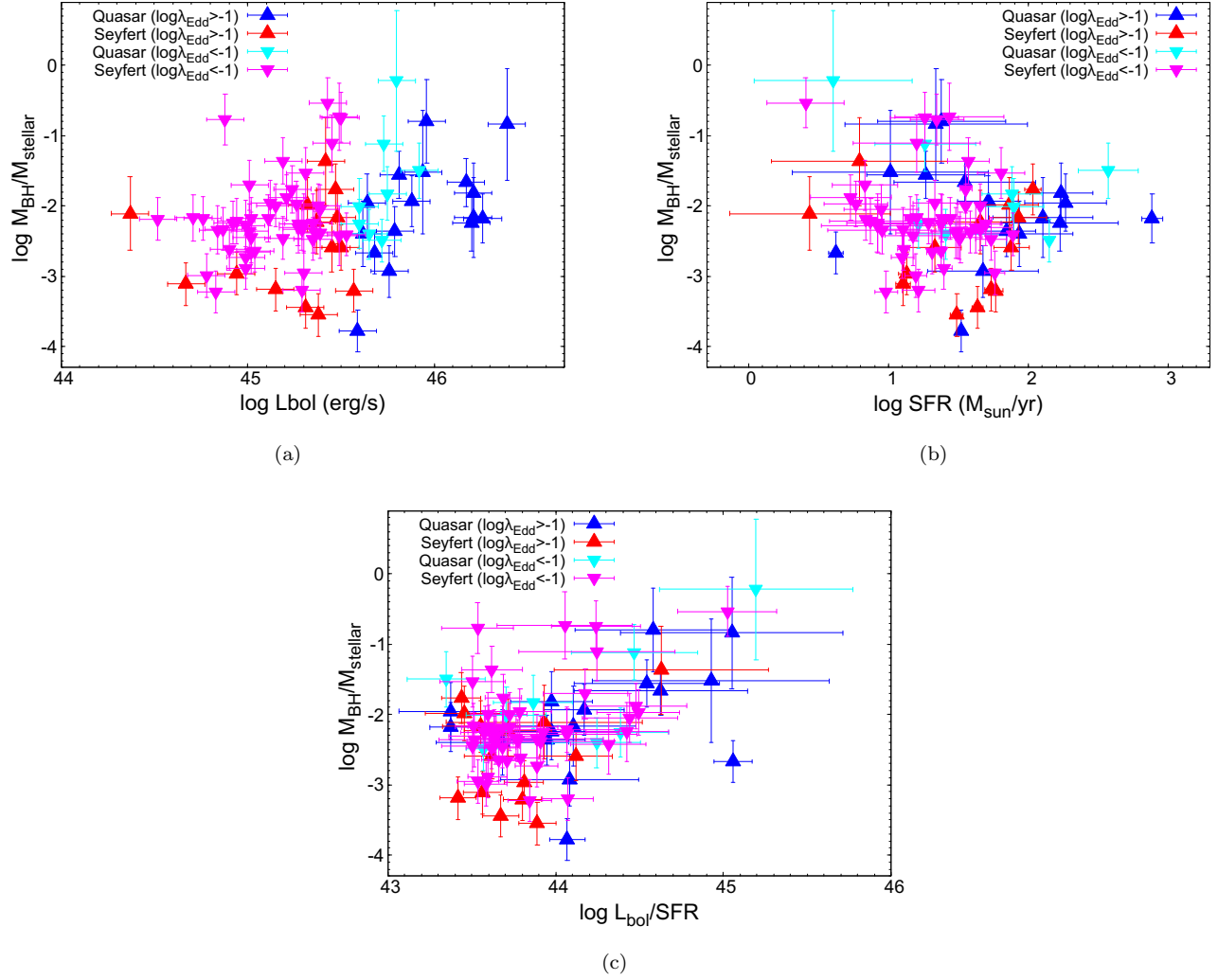


Figure 5. $M_{\text{BH}}/M_{\text{stellar}}$ plotted against (a) L_{bol} , (b) SFR, and (c) $L_{\text{bol}}/\text{SFR}$. The symbols are the same as in Figure 2.

Akiyama, M., Ueda, Y., Watson, M. G., et al. 2015, PASJ, 67, 82

Boquien, M., Burgarella, D., Roehlly, Y., et al. 2019, A&A, 622, A103

Bruzual, G., & Charlot, S. 2003, MNRAS, 344, 1000

Burgarella, D., Buat, V., & Iglesias-Páramo, J., et al. 2005, MNRAS, 360, 1413

Calzetti, D., Armus, L., Bohlin, R. C., et al. 2000, ApJ, 533, 682

Chabrier, G. 2003, PASP, 115, 763

Dale, D. A., Helou, G., Magdis, G. E., et al. 2014, ApJ, 784, 83

Gültekin, K., Richstone, D. O., Gebhardt, K., et al. 2009, ApJ, 698, 198

Håring N., & Rix, H.-W. 2004, ApJL, 604, L89

Hickox, R. C., Mullaney, J. R., Alexander, D. M., et al. 2014, ApJ, 782, 9

Inoue, A. K. 2011, MNRAS, 415, 2920

Izumi, T., Onoue, M., Matsuoka, Y., et al. 2019, PASJ, 71, 111

Jahnke, K., Bongiorno, A., Brusa, M., et al. 2009, ApJL, 706, L215

Kelly, B. C., 2007, ApJ, 665, 1489

Kocevski, D. D., Hasinger, G., Brightman, M., et al. 2018, ApJS, 236, 48

Kormendy, J., & Ho, L. C. 2013, ARA&A, 51, 511

Lonsdale, C. J., Smith, H. E., Rowan-Robinson, M., et al. 2003, PASP, 115, 897

Lonsdale, C. J., Polletta, M. d. C., Surace, J., et al. 2004, ApJS, 154, 54

Madau, P., & Dickinson, M., 2014, ARA&A, 52, 415

Magorrian, J., Tremaine, S., Richstone, D., et al. 1998, AJ, 115, 2285

Marconi, A., & Hunt, L.K., 2003, ApJ, 589, L21

- Merloni, A., Bongiorno, A., Bolzonella, M., et al. 2010, *ApJ*, 708, 137
- Nobuta, K., Akiyama, M., Ueda, Y., et al. 2012, *ApJ*, 761, 143
- Noll, S., Burgarella, D., Giovannoli, E., et al. 2009, *A&A*, 507, 1793
- Oh, K., Ueda, Y., Akiyama, M., et al. 2019, *ApJ*, 880, 112
- Oliver, S. J., Bock, J., Altieri, B., et al. 2012, *MNRAS*, 424, 1614
- Richards, G. T., Lacy, M., Storrie-Lombardi, L. J., et al. 2006, *ApJS*, 166, 470
- Rosario, D. J., Santini, P., Lutz, D., et al. 2012, *A&A*, 545, A45
- Santini, P., Rosario, D. J., Shao, L., et al. 2012, *A&A*, 540, 109
- Sawicki, M. 2012, *PASP*, 124, 1208
- Sekiguchi, K., Akiyama, M., Furusawa, H., et al. 2005, in *Multiwavelength mapping of galaxy formation and evolution*, ed. A. Renzini & R. Bender (Berlin: Springer-Verlag), 82
- Speagle, J. S., Steinhardt, C. L., Capak, P. L., et al. 2014, *ApJS*, 214, 15
- Stalevski M., Ricci C., Ueda Y., et al. 2016, *MNRAS*, 458, 2288
- Stanley, F., Harrison, C. M., Alexander, D. M., et al. 2015, *MNRAS*, 453, 591
- Stemo, A., Comerford, J. M., Barrows, R. S., et al. 2020, *ApJ*, 888, 78
- Suh, H., Civano, F., Hasinger, G., et al. 2019, *ApJ*, 872, 168
- Suh, H., Civano, F., Trakhtenbrot, B., et al. 2020, *ApJ*, 889, 32
- Toba, Y., Ueda, Y., Matsuoka, K., et al. 2019a, *MNRAS*, 484, 196
- Toba, Y., Yamashita, T., Nagao, T., et al. 2019b, *ApJS*, 243, 15
- Toba, Y., Goto, T., Oi, N., et al. 2020, *ApJ*, 899, 35
- Ueda, Y., Watson, M. G., Stewart, I. M., et al. 2008, *ApJS*, 179, 124
- Ueda, Y., Akiyama, M., Hasinger, G.;ZjZnther., et al. 2014, *ApJ*, 786, 104
- Ueda, Y., Hatsukade, B., Kohno, K., et al. 2018, *ApJ*, 853, 24
- Yang, G., Boquien, M., Buat, V., et al. 2020, *MNRAS*, 491, 740
- Yang, G., Brandt, W. N., Alexander, D. M. et al. 2019, *MNRAS*, 485, 3271
- Yang, G., Chen, C. -T. J., Vito, F., et al. 2017, *ApJ*, 842, 72
- Zhuang, M.-Y., & Ho, L. C. 2020, *ApJ*, 896, 108